MULTIBODY DYNAMICS 2003
Jorge A.C. Ambrósio (Ed.)
IDMEC/IST, Lisbon, Portugal, July 1-4 2003

AN IMPROVED ELASTO-KINEMATIC MODEL OF THE HUMAN FOREARM FOR BIOFIDELIC MEDICAL DIAGNOSIS

Andrés Kecskeméthy[†] **and Annelie Weinberg**[*]

[†] Chair for Mechanics
University Duisburg-Essen
Lotharstraße 1, D-47048 Duisburg, Germany
email: a.kecskemethy@uni-duisburg.de, web page: http://www.mechanik.uni-duisburg.de/

[*] Department for Pediatric Surgery
University of Graz
Auenbruggerplatz 34
A-8036 Graz, Austria
email: annelie.weinberg@t-online.de, web page: http://www.pediatric-surgery.at/

Keywords: Biomechanics, forearm, kinetostatics of pronation and supination.

Abstract. *Described in this paper is a new kinetostatic model of the forearm axial motion, i.e., from supination (palm up) to pronation (palm down) and vice versa. The model features an elastokinematic coupling between axial displacement and lateral swaying of the humero-ulnar (elbow) articulation. Such an evasive axial and swaying motion of the ulna has been observed by various authors using magnetic resonance imaging (MRI). In this paper, a two-degree-of-freedom model is presented in which the swaying and axial motion of the ulna is controlled by static equilibrium via two corresponding virtual springs. The spring stiffnesses are identified from geometric measurements, such that the observed motions correspond to the simulated ones. This model can be later used for biofidelic computer-oriented surgery planning. The paper presents the basic kinematic and static relationships of the model as well as an implementation featuring on-line 3D rendering of the motion of the bones.*

1 INTRODUCTION

The computer modelling of the muskuloskeletal human system is playing an increasingly important role in medicine: due to the growing number of surgical interventions as well the rising quality standards, surgeons are seeking tools that will support them in the planning of treatment types and the prediction of their consequences prior to their application. One aspect of particular interest is the axial rotation of the forearm, known also as motion from supina-

tion (palm up) to pronation (palm down). Understanding of this motion has become relevant in modern surgery due to an increasing number of corresponding treatments. For example, for children, 20% of all recorded fractures are fractures of the lower arm, thus making this the most frequent form of extremity fractures[1]. For the treatment of such lower arm fractures, there exist two methods[2]. In the operative form of treatment, the bone fragments are fixed by mechanical aids. In the conservative therapy, the bone fragments are re-positioned without surgical intervention (the preferred therapy form for children). Experience shows that both methods often result in functional deficiencies that usually affect the rotational movement of the lower arm[3]. These deficiencies arise due to misalignments of bone fragments after healing which may lead to a pathological contact between the two bones of the forearm that obstructs further motion. Current literature gives evidence that elimination of such functional deficiencies will entail an increase in the number of operations as initial treatment, which implies also an increase of economic costs. Whereas the operation rate prior to the 90's was, on average, between 3-7%, recent studies have recorded the actual rate to be 4% to 14%[4] or even 23,3%[5]. Methods that help surgeons to assess *a priori* the consequences of such operative interventions will help either to reduce surgical intervention and thus stress on the children or, if such interventions become unavoidable, allow these to be constrained to a minimum. A computer program that allows one to relate the degree of possible misalignment between the bone fragment axes after healing and pro-/supination function limitations would provide an important tool for (1) deciding whether a corrective surgery is necessary at all, or (2), in the case a correction is necessary, give a clue on how to do the minimally possible correction such that no impairment of function will occur.

In order for such a computer program to be applicable in practice, it must fulfill two requirements: (1) it must render precise enough predictions of the forearm motion such that they can be employed for surgical planning, and (2) it must carry out the computations fast enough such that an online motion simulation is possible. To this end, the complex interrelationships between bones, joints and ligaments are reduced to a few characteristic motion quantities which reproduce the target motion in a sufficiently accurate way. The objective is to find a multibody model which, although possibly built differently than the target system, reproduces the behaviour of the real system accurately enough, and, by using the methodologies developed for mechanical systems, does this simulation in very short time. Such surrogate mechanisms have been developed for other human joints, such as the four-bar surrogate mechanism of Menschik for the human knee[6], or the hexapod surrogate mechanism proposed by one of the authors for reproducing the force-motion behaviour at the human cervical spine[7].

Proposed in this paper is a novel surrogate mechanism for pro- and supination motion that takes into account perturbations of the ideal hinge motion of ulna with respect to humerus by introducing two additional degrees of freedom at the humero-ulnar articulation: (1) a lateral (outward) sway of the ulna bone, and (2) an axial translation of the ulna bone. Although these two degrees of freedom are only activated by small amounts, they have large effect on gross motion of the forearm bones and thus become significant for a realistic prediction of the forearm motion. For the actuation of these two degrees of freedom, we propose a new "kinetostatic" method in which virtual springs are introduced for both degrees of freedom and the motion of

the system is determined as a sequence of equilibrium configurations for varying outer torque loading. By fitting the resulting simulated motion to the measured motion, the stiffness coefficients can be determined, yielding a compliant model that reproduces the motion accurately. In this way one obtains an example of applicability of methods for multibody systems and mechanism analysis to biomechanical problems.

The rest of the paper is organized as follows. Section 2 describes the basic anatomic units involved in the pro- and supination motion, as well as the basic kinematic surrogate models encountered in the literature. In Section 3, the extended model using two degrees of freedom and the concept for determining the unknown spring stiffness coefficients are presented. The preliminary results obtained for the fitting of this model to anatomical data are discussed in Section 4. These are limited here to a single-specimen verification, which are intended to be generalized to comprehensive tests for model validation in future works.

2 BASIC FUNCTIONAL PROPERTIES OF PRO- AND SUPINATION

In the axial rotation of the forearm, two bones *ulna* (at the small finger side) and *radius* (at the thumb side) are involved (Fig. 1). The forearm bones are held together trough a complex set of ligaments that restrict their relative motion to a more or less torsional motion of the radius around the ulna. Shown in Fig. 1 is the basic structure of the forearm bones and ligaments for the

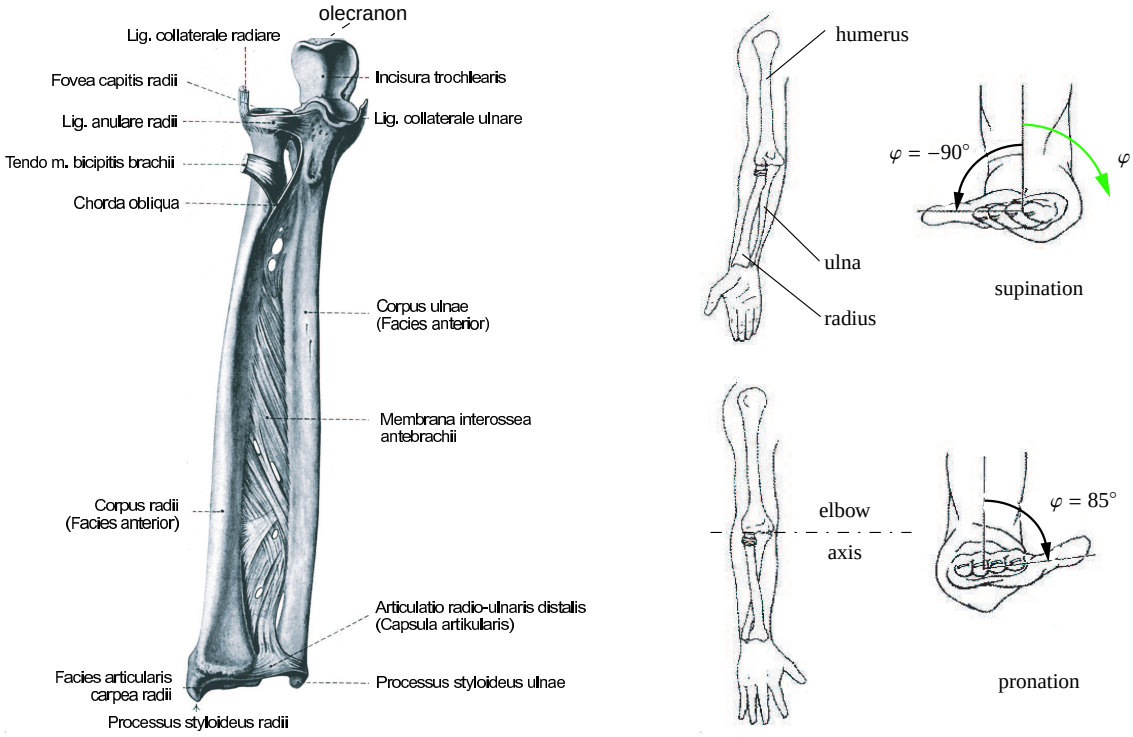

Figure 1: Anatomy of the forearm bones [adapted from Rauber and Kopsch[8] and Kapandji[9]]

right arm in the palm-up (supination) position. Hereby, the upper (proximal) end corresponds to the elbow and the lower (distal) end corresponds to the wrist. For the kinematics of pro- and supination motion, two kinds of displacements are relevant: (1) the displacements between the two forearm bones and the humerus; and (2) the relative motion between the two forearm bones.

Regarding the motion of the forearm bones with respect to humerus, classical anatomy makes two basic assumptions: (1.1) the spherical concave shape of the proximal articulation of the radius (the *fovea capitis radii*) allows the radius to perform a fixed-point, i.e., spherical rotation about the correspondingly shaped surface of the humerus (termed the *condyle*), while (1.2) the clamp-shaped *olecranon* of the ulna at its proximal end firmly grasps the corresponding surface of the humeral side of the articulation and allows only a rotation about the elbox axis. Thus, in the classical elbow model, the ulna is assumed to be fixed with respect to the humerus during pro- and supination.

Concerning the relative motion between the two forearm bones, one recognizes two contact locations between radius and ulna, termed the proximal and distal radioulnar joints, respectively. In classical anatomy, these contact locations are regarded as spherical articulations, respectively, due to the correspondingly shaped contact surfaces[10] (see Fig. 2). Hereby, in the proximal

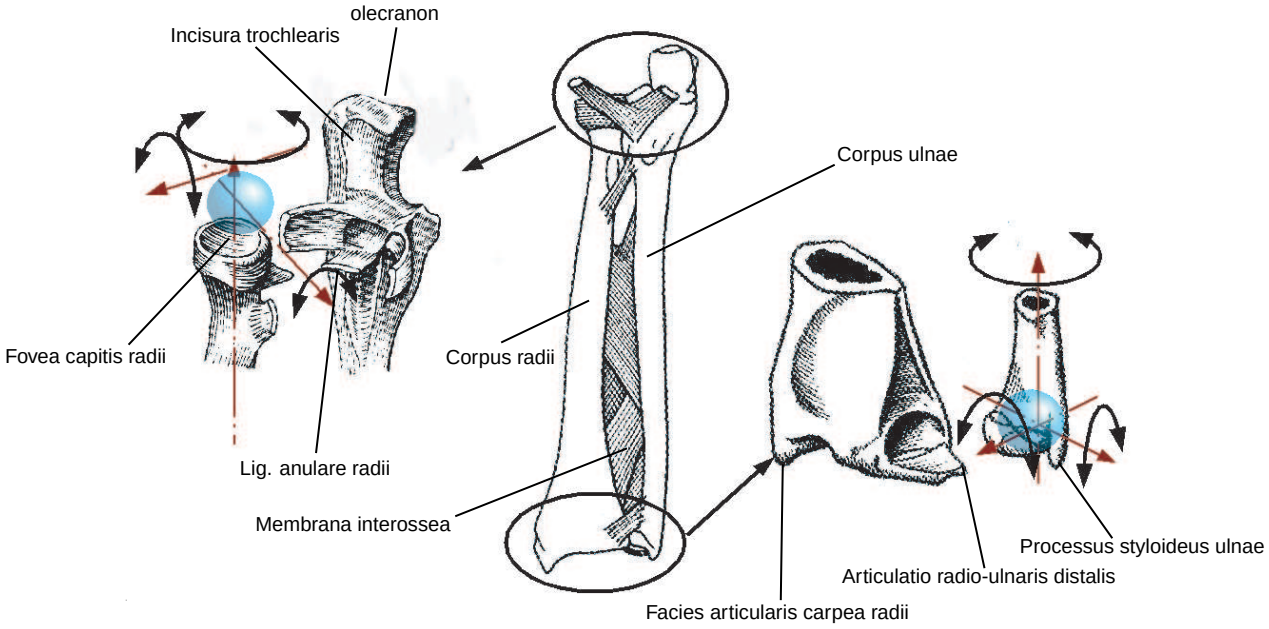

Figure 2: Basic modeling of relative motion between ulna and radius

articulation, the two ends of radius and ulna are pressed together by a circular ligament, the *ligamentum annulare radii*, while at the distal end the two ends of the bones are held together through an oblique ligament, the *ligamentum collaterale ulnare*. Moreover, both bones are held together by a cross-fibered membrane termed the *membrana interossea antebracii*. As a

result, classical theory predicts for the pure pro- and supination motion a fixed ulna and a pure rotation of the radius about a fixed axis that passes through the two centers of the spherical articulations modelling the contact locations between ulna and radius (Fig. 3a). The problem

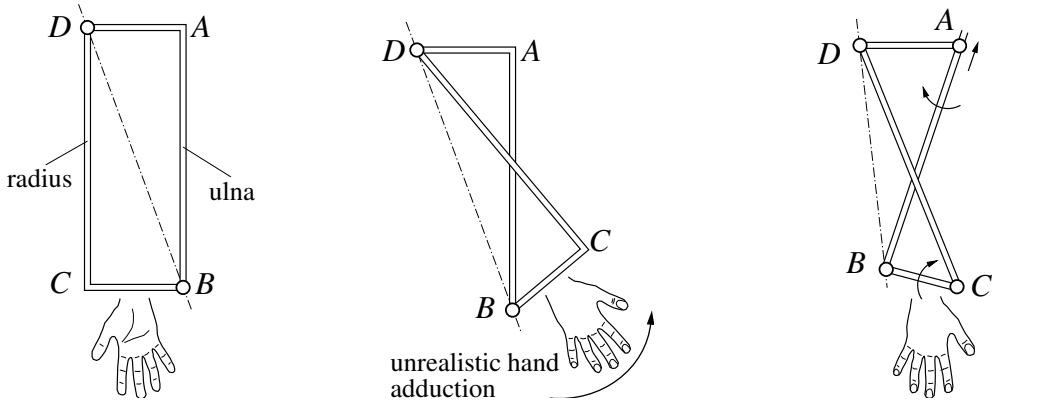

a) supination b) tilting of hand in pronation c) compensation of tilting

Figure 3: Deficiencies of the spherical-spherical model

with this spherical-spherical model is that it renders an unrealistic strong tilting of the wrist from supination to pronation (Fig. 3b). In fact, as has been verified by MRI measurements by Kapandji[9], Nakamura et al.[11], and Weinberg[12], during pro- and supination motion the ulna is not fixed with respect the humerus but performs a small swaying (lateral) motion as well as a small axial sliding along its axis with respect to the humerus bone (Fig. 3c). By this swaying and axial displacement motion, the tilting angle of the wrist can be reduced. However, in order to be able to rotate the radius outwards, one must compensate the thus arising length change between *A* and *B*. This can happen only by an axial displacement at the humero-ulnar joint, or by an additional joint at *C*[13]. As pure dislocation compensation leads to an exaggerated axial displacement at the elbow[14], one infers that a revolute joint must be present at *C*. Such a joint can be found as a virtual rotation center within the radius corpus (Fig. 4). This joint is not

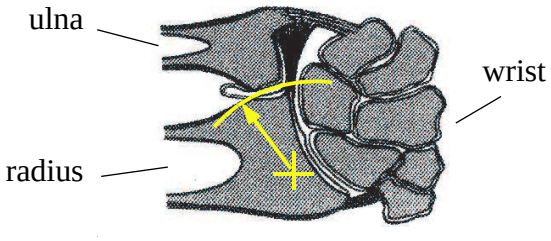

Figure 4: Virtual rotation center at distal radius head.

a *physical* articulation but represents the center of curvature of the projection of the contact

surface between radius and ulna at the distal radio-ulnear articulation on the plane spanned by ulna axis and distal radioulnar contact point.

3 SURROGATE MECHANISM FOR PRO- AND SUPINATION

By combining the individual elements discussed above, the surrogate mechanism displayed in Fig. 5 arises. This is a PR-H-R-S mechanism, where P, R, H and S represent a prismatic, revolute, Hooke and spherical joint, respectively. Here, $\underline{r}_1$, $\underline{r}_2$, $\underline{r}_3$, $\underline{r}_4$ denote the ulna, the wrist, the radius, and the elbow vectors, respectively, while P and R_ϑ contain the axial displacement s and lateral swaying ϑ of the ulna with respect to the humerus, respectively; H is a Hooke's joint embodying the pro-/supination angle φ and the torsional angle ψ_1 between radius and ulna, R_2 is the joint at the virtual transversal rotation center between radius and ulna describing the aperture ψ_2 between ulna and radius, and S is the spherical joint representing the fixed-point rotation of radius with respect to humerus, represented, e.g., by roll-pitch-roll angles $\gamma_1, \gamma_2, \gamma_3$. This mechanism has two degrees of freedom, represented in Fig. 5 by s and φ. To make static equilibrium under loading possible, at least one virtual spring per degree of freedom is required. These two virtual springs summarize all elasticity effects acting between the two forearm bones as well as the humerus, including ligaments, capsules, etc. The two springs are placed here at the humeroulnar articulation with respect to axial and swaying displacement, respectively. The corresponding spring stiffnesses c_s and c_ϑ are determined in the present approach from the fitting of the model to the measured displacements of ulna during pro- and supination. Other approaches could foresee determining the spring stiffnesses directly by MRI measurements of the bone motion under physiologic loadings.

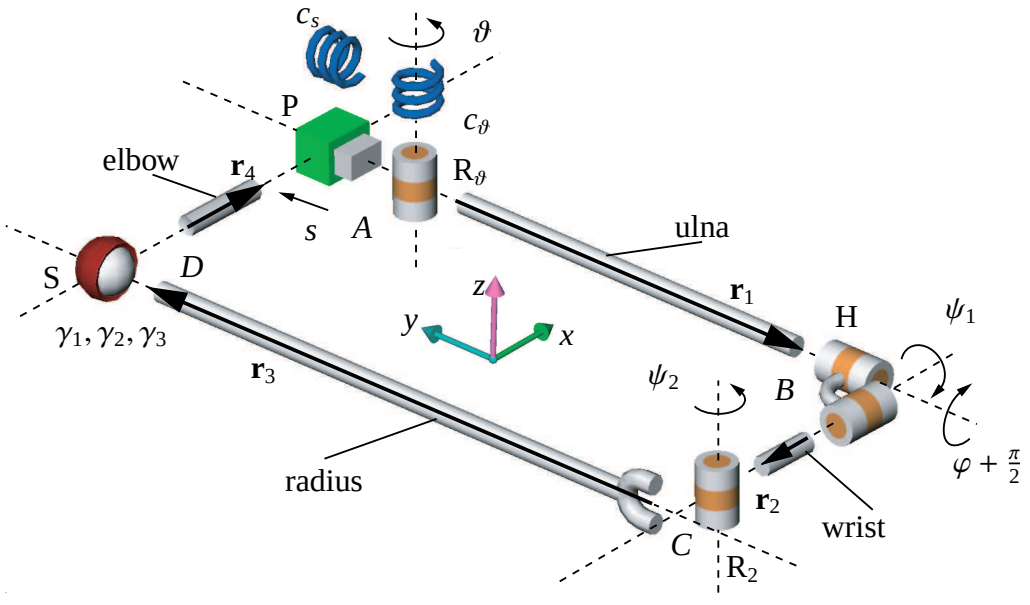

Figure 5: Two-degrees-of-freedom surrogate mechanism for pro- and supination

3.1 Position Kinematics

The kinematics of the surrogate mechanism can be compactly described using homogeneous vectors and corresponding homogeneous transformation matrices for representing rigid-body motions[15]. Hereby, we introduce the notation

$$\overset{\mathrm{H}}{\underline{p}} = \begin{bmatrix} p_x \\ p_y \\ p_z \\ 1 \end{bmatrix} \tag{1}$$

for homogeneous coordinates and

$$\mathbf{A} = \begin{bmatrix} \mathbf{R} & \underline{r} \\ 0 & 1 \end{bmatrix} = \begin{bmatrix} \rho_{11} & \rho_{12} & \rho_{13} & r_x \\ \rho_{21} & \rho_{22} & \rho_{23} & r_y \\ \rho_{31} & \rho_{32} & \rho_{33} & r_z \\ 0 & 0 & 0 & 1 \end{bmatrix} \tag{2}$$

for homogeneous matrices, where $\underline{p} = [p_x, p_y, p_z]^{\mathrm{T}}$ is a general vector in 3D space, while $\mathbf{R}$ is the orthogonal rotation matrix with components ρ_{ij} describing, columnwise, the representation of the rotated coordinate unit vectors in the base frame, and $\underline{r}$ is the displacement vector with components r_{xyz} desribing the location of the origin of the moving frame in coordinates of the base frame. Rigid-body motion is represented by the transformation of body-fixed coordinates $\underline{p}' = [p_{x'}, p_{y'}, p_{z'}]^{\mathrm{T}}$ with respect to the moving frame to fixed coordinates $\underline{p} = [p_x, p_y, p_z]^{\mathrm{T}}$ with respect to the base frame

$$\begin{bmatrix} \underline{p} \\ 1 \end{bmatrix} = \begin{bmatrix} \mathbf{R} & \underline{r} \\ 0 & 1 \end{bmatrix} \begin{bmatrix} \underline{p}' \\ 1 \end{bmatrix} \ . \tag{3}$$

In particular, one can introduce the elementary transformations

$$\mathtt{Rot}[\,\underline{e}_1, \Theta\,] = \begin{pmatrix} 1 & 0 & 0 & 0 \\ 0 & \cos\Theta & -\sin\Theta & 0 \\ 0 & \sin\Theta & \cos\Theta & 0 \\ 0 & 0 & 0 & 1 \end{pmatrix} \quad , \quad \mathtt{Trans}[\,\underline{e}_1, s\,] = \begin{pmatrix} 1 & 0 & 0 & s \\ 0 & 1 & 0 & 0 \\ 0 & 0 & 1 & 0 \\ 0 & 0 & 0 & 1 \end{pmatrix} \ , \tag{4a}$$

$$\mathtt{Rot}[\,\underline{e}_2, \Theta\,] = \begin{pmatrix} \cos\Theta & 0 & \sin\Theta & 0 \\ 0 & 1 & 0 & 0 \\ -\sin\Theta & 0 & \cos\Theta & 0 \\ 0 & 0 & 0 & 1 \end{pmatrix} \quad , \quad \mathtt{Trans}[\,\underline{e}_2, s\,] = \begin{pmatrix} 1 & 0 & 0 & 0 \\ 0 & 1 & 0 & s \\ 0 & 0 & 1 & 0 \\ 0 & 0 & 0 & 1 \end{pmatrix} \ , \tag{4b}$$

$$\mathtt{Rot}[\,\underline{e}_3, \Theta\,] = \begin{pmatrix} \cos\Theta & -\sin\Theta & 0 & 0 \\ \sin\Theta & \cos\Theta & 0 & 0 \\ 0 & 0 & 1 & 0 \\ 0 & 0 & 0 & 1 \end{pmatrix} \quad , \quad \mathtt{Trans}[\,\underline{e}_3, s\,] = \begin{pmatrix} 1 & 0 & 0 & 0 \\ 0 & 1 & 0 & 0 \\ 0 & 0 & 1 & s \\ 0 & 0 & 0 & 1 \end{pmatrix} \tag{4c}$$

where $\underline{e}_i$ denote the unit vectors in direction of the three coordinate axes, respectively, Θ is a rotation angle, and s is a translation. Moreover, one can introduce for pure rotation and pure translation the shortcuts

$$\texttt{Rot}[\,\mathbf{R}\,] = \begin{bmatrix} \mathbf{R} & \underline{0} \\ 0 & 1 \end{bmatrix} \;;\; \texttt{Trans}[\,\underline{r}\,] = \begin{bmatrix} \mathbf{I}_3 & \underline{r} \\ 0 & 1 \end{bmatrix} , \tag{5}$$

where $\mathbf{I}_n$ denotes a $n \times n$ identity matrix. Then, one can write for the loop closure condition

$$\begin{aligned} &\texttt{Trans}[\,y, s\,] \circ \texttt{Rot}[\,z, \vartheta\,] \circ \texttt{Trans}[\,\underline{r}_1\,] \circ \texttt{Rot}[\,y, \varphi + \pi/2\,] \circ \texttt{Rot}[\,x, \psi_1\,] \circ \texttt{Trans}[\,\underline{r}_2\,] \\ &\circ \texttt{Rot}[\,z, \psi_2\,] \circ \texttt{Trans}[\,\underline{r}_3\,] \circ \texttt{Rot}[\,y, \gamma_1\,] \circ \texttt{Rot}[\,z, \gamma_2\,] \circ \texttt{Rot}[\,x, \gamma_3\,] \circ \texttt{Trans}[\,\underline{r}_4\,] = \mathbf{I}_4 \end{aligned} \tag{6}$$

where $\circ$ is the composition operator describing the concatenation of two subsequent transformations. By re-ordering the individual transformations in Eq. (6), and taking into account that

$$\mathbf{A}^{-1} = \begin{bmatrix} \mathbf{R}^{\mathrm{T}} & -\mathbf{R}^{\mathrm{T}}\,\underline{r} \\ 0 & 1 \end{bmatrix} \tag{7}$$

one can write as an alternative loop closure condition, after taking into account that $\texttt{Trans}[\,-\underline{r}_2\,]$ and $\texttt{Rot}[\,x, \psi_1\,]$ commute for the particular geometry at hand,

$$\begin{aligned} &\texttt{Rot}[\,x, \psi_1\,] \circ \texttt{Rot}[\,z, \psi_2\,] \circ \texttt{Trans}[\,\underline{r}_3\,] \circ \texttt{Rot}[\,y, \gamma_1\,] \circ \texttt{Rot}[\,z, \gamma_2\,] \circ \texttt{Rot}[\,x, \gamma_3\,] \\ &= \texttt{Trans}[\,-\underline{r}_2\,] \circ \texttt{Rot}[\,y, -(\varphi + \pi/2)\,] \circ \texttt{Trans}[\,-\underline{r}_1\,] \circ \texttt{Rot}[\,z, -\vartheta\,] \circ \texttt{Trans}[\,y, -s\,] \\ &\quad \circ \texttt{Trans}[\,-\underline{r}_4\,] \;. \end{aligned} \tag{8}$$

This equation describes that the transformation from the wrist point C (after commutation of $\texttt{Trans}[\,-\underline{r}_2\,]$ and $\texttt{Rot}[\,x, \psi_1\,]$ now also including the rotation by ψ_1) to the humero-radial joint S can be described either through the sequence $\psi_1, \psi_2, \underline{r}_3, \gamma_1, \gamma_2, \gamma_3$, or through the sequence $-\underline{r}_2, -\varphi, -\underline{r}_1, -\vartheta, -s, -\underline{r}_4$. Assuming all vectors to be coplanar in the supination (palm up) position, one can set

$$\underline{r}_1 = \begin{bmatrix} 0 \\ -r_1 \\ 0 \end{bmatrix} \;;\; \underline{r}_2 = \begin{bmatrix} -r_2 \\ 0 \\ 0 \end{bmatrix} \;;\; \underline{r}_3 = \begin{bmatrix} 0 \\ r_3 \\ 0 \end{bmatrix} \;;\; \underline{r}_4 = \begin{bmatrix} r_4 \\ 0 \\ 0 \end{bmatrix} \tag{9}$$

and the matrix coefficients of Eq. (8) become

$$\begin{bmatrix} 1 & 0 & 0 & r_2 \\ 0 & 1 & 0 & 0 \\ 0 & 0 & 1 & 0 \\ 0 & 0 & 0 & 1 \end{bmatrix} \cdot \begin{bmatrix} -\sin\varphi & 0 & -\cos\varphi & 0 \\ 0 & 1 & 0 & 0 \\ \cos\varphi & 0 & -\sin\varphi & 0 \\ 0 & 0 & 0 & 1 \end{bmatrix} \cdot \begin{bmatrix} 1 & 0 & 0 & 0 \\ 0 & 1 & 0 & r_1 \\ 0 & 0 & 1 & 0 \\ 0 & 0 & 0 & 1 \end{bmatrix} \cdot$$
$$\begin{bmatrix} \cos\vartheta & \sin\vartheta & 0 & 0 \\ -\sin\vartheta & \cos\vartheta & 0 & 0 \\ 0 & 0 & 1 & 0 \\ 0 & 0 & 0 & 1 \end{bmatrix} \cdot \begin{bmatrix} 1 & 0 & 0 & 0 \\ 0 & 1 & 0 & -s \\ 0 & 0 & 1 & 0 \\ 0 & 0 & 0 & 1 \end{bmatrix} \cdot \begin{bmatrix} 1 & 0 & 0 & -r_4 \\ 0 & 1 & 0 & 0 \\ 0 & 0 & 1 & 0 \\ 0 & 0 & 0 & 1 \end{bmatrix}$$
$$= \begin{bmatrix} 1 & 0 & 0 & 0 \\ 0 & \cos\psi_1 & -\sin\psi_1 & 0 \\ 0 & \sin\psi_1 & \cos\psi_1 & 0 \\ 0 & 0 & 0 & 1 \end{bmatrix} \cdot \begin{bmatrix} \cos\psi_2 & -\sin\psi_2 & 0 & 0 \\ \sin\psi_2 & \cos\psi_2 & 0 & 0 \\ 0 & 0 & 1 & 0 \\ 0 & 0 & 0 & 1 \end{bmatrix} \cdot \begin{bmatrix} 1 & 0 & 0 & 0 \\ 0 & 1 & 0 & r_3 \\ 0 & 0 & 1 & 0 \\ 0 & 0 & 0 & 1 \end{bmatrix} \cdot \begin{bmatrix} & \mathbf{R}_S & & 0 \\ & & & 0 \\ & & & 0 \\ 0 & 0 & 0 & 1 \end{bmatrix} \tag{10}$$

where $\mathbf{R}_S = \mathbf{R}(\gamma_1, \gamma_2, \gamma_3)$ is the rotation matrix at the spherical joint. From this matrix equation, one can extract proper scalar equations for determination of the three unknowns φ (pro- and supination angle), ψ_1 (torsional angle between ulna and radius) and ψ_2 (aperture angle) between ulna and radius. Eq. (10) contains 12 nonvanishing equations, from which six are independent. As the mechanism features 8 elementary degrees of freedom at the joints, described by the variables $\underline{\beta} = [s, \vartheta, \varphi, \psi_1, \psi_2, \gamma_1, \gamma_2, \gamma_3]^{\mathrm{T}}$, the loop has $8 - 6 = 2$ degrees of freedom, which are chosen here as s and φ. Due to the particular geometry of the loop, the six remaining variables can be determined in closed-form as functions of the two degrees of freedom. An approach for automatically finding a suitable sequence of equations such that a closed-form solution can be found is proposed by Kecskemethy and Hiller[16]. Although the equations can be obtained also "by inspection", we briefly apply this approach to the present problem, as it sheds some light on the geometric nature of the individual equations.

First, regard that by computing the variables $\vartheta, \psi_1, \psi_2$, the position of all bodies of the loop can be determined. Hence, the spherical joint angles $\gamma_1, \gamma_2, \gamma_3$ are not required. Suitable scalar equations can be obtained from Eq. (10) by multiplication from the right and the left with pairs of basis vectors

$$\overset{\mathrm{H}}{\underline{e}}_1 = \begin{bmatrix} 1 \\ 0 \\ 0 \\ 0 \end{bmatrix}, \quad \overset{\mathrm{H}}{\underline{e}}_2 = \begin{bmatrix} 0 \\ 1 \\ 0 \\ 0 \end{bmatrix}, \quad \overset{\mathrm{H}}{\underline{e}}_3 = \begin{bmatrix} 0 \\ 0 \\ 1 \\ 0 \end{bmatrix}, \quad \overset{\mathrm{H}}{\underline{o}} = \begin{bmatrix} 0 \\ 0 \\ 0 \\ 1 \end{bmatrix}. \tag{11}$$

Here, vectors $\overset{\mathrm{H}}{\underline{e}}_i, i = 1, 2, 3$ represent geometrically the three orientation vectors in direction of the coordinate axes, or, respectively, normal to the coordinate planes, and $\overset{\mathrm{H}}{\underline{o}}$ is the position vector representing the origin of the coordinate system. Note that, for orientation vectors, one can verify the relationship

$$\mathbf{A}^{-1} \overset{\mathrm{H}}{\underline{e}} = \mathbf{A}^{\mathrm{T}} \overset{\mathrm{H}}{\underline{e}}. \tag{12}$$

Due to this property, multiplication from the left of a homogeneous matrix is defined for an orientation vector:

$$\overset{\mathrm{H}}{\underline{u}}\,{}^{\mathrm{T}}\mathbf{A} = \left(\mathbf{A}^{\mathrm{T}}\,\overset{\mathrm{H}}{\underline{u}}\right)^{\mathrm{T}} = \left(\mathbf{A}^{-1}\,\overset{\mathrm{H}}{\underline{u}}\right)^{\mathrm{T}} . \tag{13}$$

For positional vectors, one can define the 'homogeneous norm'

$$\|\,\underline{\xi}\,\|_{\mathrm{H}} = \sqrt{\|\,\underline{\xi}\,\|^2 - 1}\ , \tag{14}$$

where $\|\ \cdot\ \|$ denotes the Euclidean norm. It holds

$$\|\mathbf{A}\ \overset{\mathrm{H}}{\underline{o}}\ \|_{\mathrm{H}} = \|\mathbf{A}^{-1}\ \overset{\mathrm{H}}{\underline{o}}\ \|_{\mathrm{H}} . \tag{15}$$

This equation expresses the fact that the distance between the origins of a fixed and a moving frame is independent of the direction of transformation.

Multiplying Eq. (10) with $\overset{\mathrm{H}}{\underline{o}}$ from the right taking the homogeneous norm clearly eliminates the effects of the spherical joint as well as the two rotations ψ_1 and ψ_2. This expresses that the distance between the center of the spherical joint and the radial-side intersection point of the two axes for ψ_1 and ψ_2 does not depend on the corresponding joint variables. Equating the square of the homogeneous norms on both sides yields for the remaining unknown ϑ the equation

$$A(s,\varphi)\,\cos\vartheta + B(s,\varphi)\,\sin\vartheta + C(s) = 0\ ,\ \text{where}\ \left\{\begin{array}{rcl} A &=& 2\,(r_2\,r_4\,\sin\varphi - r_1\,s) \\ B &=& 2\,(r_2\,s\,\sin\varphi - r_1\,r_4) \\ C &=& r_1^2 + r_2^2 + r_4^2 + s^2 - r_3^2 \end{array}\right. \tag{16}$$

This equation can be rewritten as

$$\overline{C}\,\cos(\vartheta - \vartheta^*) + C = 0\ ,\ \text{where}\ \overline{C} = \sqrt{A^2 + B^2}\ ,\ \tan\vartheta^* = \frac{B}{A}\ , \tag{17}$$

yielding the solution $\vartheta(s,\varphi) = \vartheta^* \pm \cos^{-1}(C/\overline{C})$. Along the same token, multiplying Eq. (10) from the right with $\overset{\mathrm{H}}{\underline{o}}$ and from the left with $\overset{\mathrm{H}}{\underline{e}}_1$, eliminates the rotations at the spherical joint as well as the rotation ψ_1. The reason is that this multiplication computes the distance between the center of the spherical joint and the plane perpendicular to the axis of the rotation ψ_1, which do not depend on the unkowns $\gamma_1, \gamma_2, \gamma_3$ and ψ_1, respectively. Thus, one obtains for the angle ψ_2

$$\sin\psi_2 = -\frac{r_2 + \sin\varphi\,(r_4\,\cos\vartheta + s\,\sin\vartheta)}{r_3}\ . \tag{18}$$

Finally, multiplying Eq. (10) from the right with $\overset{\mathrm{H}}{\underline{o}}$ and from the left with $\overset{\mathrm{H}}{\underline{e}}_2$ and $\overset{\mathrm{H}}{\underline{e}}_3$, respectively, yields the two equations

$$r_3\,\cos\psi_1\ \cos\psi_2 \;=\; r_1 + r_4\,\sin\vartheta - s\,\cos\vartheta \tag{19a}$$

$$r_3\,\sin\psi_1\ \cos\psi_2 \;=\; \cos\varphi\,(\,r_4\,\cos\vartheta + s\,\sin\vartheta\,) \tag{19b}$$

from which it follows

$$\tan\psi_1 = -\frac{\cos\varphi\,(\,r_4\,\cos\vartheta + s\,\sin\vartheta\,)}{r_1 + r_4\,\sin\vartheta - s\,\cos\vartheta}\ . \tag{19c}$$

Hence, all three angles $\vartheta, \psi_1, \psi_2$ can be computed as (explicit) functions of the two degrees of freedom s and φ.

3.2 Velocity Relationships

For the kinetostatic modeling described below, the Jacobian of the transmission from degrees of freedom to the pro- and supination angle φ is needed. To this end, note that from the time-derivative of Eq. (16) it follows

$$A_\vartheta\,\dot{\vartheta} + A_s\,\dot{s} + A_\varphi\,\dot{\varphi} = 0 \ , \tag{20a}$$

where

$$\left\{\begin{array}{lcl} A_\vartheta &=& r_4\,(\,r_1\,\cos\vartheta - r_2\,\sin\vartheta\sin\varphi\,) + s\,(\,r_2\,\cos\vartheta\sin\varphi + r_1\,\sin\vartheta\,) \\ A_s &=& r_2\,\sin\vartheta\sin\varphi + r_1\,\cos\vartheta \\ A_\varphi &=& r_2\,(\,r_4\,\cos\vartheta + s\,\sin\vartheta\,)\cos\varphi \end{array}\right. \tag{20b}$$

From this one obtains

$$\dot{\vartheta} = \left[J_s\ ,\ \ J_\varphi\right]\left[\begin{array}{c}\dot{s}\\ \dot{\varphi}\end{array}\right] = \mathbf{J}\,\underline{\dot{q}} \tag{21a}$$

where $\mathbf{J} = [J_s, J_\varphi]$ is the Jacobian of the transmission, $\underline{q} = [s, \varphi]^{\mathrm{T}}$ is the vector of input coordinates, and for the coefficients J_s, J_φ of the Jacobian $\mathbf{J}$ it holds

$$J_s \;=\; -\frac{A_s}{A_\vartheta} = -\frac{r_2\,\sin\vartheta\sin\varphi + r_1\,\cos\vartheta}{r_4\,(\,r_1\,\cos\vartheta - r_2\,\sin\vartheta\sin\varphi\,) + s\,(\,r_2\,\cos\vartheta\sin\varphi + r_1\,\sin\vartheta\,)} \ , \tag{21b}$$

$$J_\varphi \;=\; -\frac{A_\varphi}{A_\vartheta} = -\frac{r_2\,(\,r_4\,\cos\vartheta + s\,\sin\vartheta\,)\cos\varphi}{r_4\,(\,r_1\,\cos\vartheta - r_2\,\sin\vartheta\sin\varphi\,) + s\,(\,r_2\,\cos\vartheta\sin\varphi + r_1\,\sin\vartheta\,)} \ . \tag{21c}$$

For typical parameters of the forearm, it holds $\vartheta << 1$, hence the denominator is always positive and the transmission is free from singularities. On the other hand, note that for supination $\varphi = -\pi/2$ and pronation $\varphi = \pi/2$ the Jacobian coefficient J_φ vanishes. Hence, the model suggests that at supination and pronation the swaying of the ulna is "locked" with respect to axial rotation of the forearm, i.e, lateral forces do not produce a tendency to pronation, while for other axial rotations they do.

3.3 Kinetostatics

In the kinematical analysis of the forearm mechanism, motion is prescribed by the two degrees of freedom at the humero-ulnar joint. However, for pro- and supination motion, one typically prescribes the pronation angle φ, i.e., the rotation about the ulnar axis, and seeks the ensuing motion at the other joints. As there are two degrees of freedom, the distribution of the pronation rotation on the individual relative joint motions and thus of the bones is not unique. In order to find a suitable relationship for these small perturbations, one can imagine that, at the two humeroulnar joints, virtual springs with unknown stiffness coefficients c_s, c_ϑ, respectively, are placed, and that the motion is prescribed by a torque applied in direction of the pronation angle, such as if a third person would try to twist one's hand by applying an external moment about the midfinger. Then, depending on the ratio of the two spring stiffnesses c_s, c_ϑ, either the

one or the other degree of freedom will be more deflected. By comparing the computed tilting angle with the measured one, one can find a stiffness ratio which reproduces the observed geometric motion. Thus one defines in this way a solution to the problem of finding minor two-degree-of-freedom actuation by measuring a global gross motion behaviour.

For the force transmission, there holds a very simple relationship which is the dual of the velocity transmission. As shown in Kecskemethy[17], this relationship follows by regarding the mechanism as a kinetostatic transmission element transmitting both motion and forces in an ideal manner, i.e., without increase or decrease of power (Fig. 6). Let the force at the prismatic

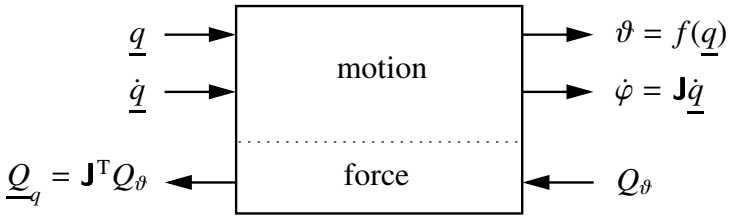

Figure 6: Model of the kinetostatic transmission element

joint P be Q_s and the torque about the revolute joint R_ϑ be Q_ϑ. Moreover, let Q_φ be the torque about the pronation rotation φ, and collect the force and torque at the input joints in a vector $\underline{Q}_q = [Q_s, Q_\varphi]^{\mathrm{T}}$. Then, equality of power at input and output requires

$$\underline{Q}_q^{\mathrm{T}}\, \dot{\underline{q}} = Q_\vartheta\, \dot{\vartheta} \quad . \tag{22}$$

Inserting here the kinematical relationship (21a) for $\dot{\varphi}$ yields

$$\underline{Q}_q^{\mathrm{T}}\, \dot{\underline{q}} = Q_\vartheta\, \mathbf{J}\, \dot{\underline{q}} \quad .$$

As this relationship must hold for any input velocity, the coefficients of $\dot{\underline{q}}$ on both sides of the equations must equate and one obtains the transmission of forces as

$$\underline{Q}_q = \mathbf{J}^{\mathrm{T}}\, Q_\vartheta \quad , \tag{23}$$

which is performed by the transposed Jacobian in opposite direction to the velocities.

Due to the compliance of the two virtual springs, forces and torques applied at the forearm mechanism will induce a deflection at the joints at which the springs are placed. A simple control moment along the pronation axis can be generated by introducing an additional spring law of the form

$$Q_\varphi = c_\varphi\, (\varphi - \varphi^*) \quad , \tag{24a}$$

where φ^* and c_φ are a (changing) user-supplied input value describing the offset of the deflection and the stiffness of a torsional spring acting about the pronation axis, respectively. At the

humeroulnar degrees of freedom, it holds $Q_s = c_s\, s$ and $Q_\vartheta = c_\vartheta\, \vartheta$. Inserting these relationships in Eq. (23) yields two nonlinear equations

$$c_\varphi\,(\varphi - \varphi^*) \;=\; J_\varphi\, c_\vartheta\, \vartheta \;, \tag{24b}$$

$$c_s\, s \;=\; J_s\, c_\vartheta\, \vartheta \;. \tag{24c}$$

These equations can be solved by a Newton-Raphson solver for given input value φ^*, yielding the three variables φ, ϑ, s, and hence the position of static equilibrium corresponding to the input value φ^*. By varying φ^*, one obtains a sequence of equilibrium positions $s(\varphi^*), \vartheta(\varphi^*), \varphi(\varphi^*)$ that can be resolved (numerically) for φ. Thus, one can construct computed functions $s_C(\varphi)$ and $\vartheta_C(\varphi)$ which describe the deflections at the degrees of freedom for a given pronation angle. These computed functions $s_C(\varphi)$ and $\vartheta_C(\varphi)$ depend on the chosen stiffness coefficients. These coefficients can be determined such that the computed functions match measured functions $s_M(\varphi)$ and $\vartheta_M(\varphi)$ in a best-fit manner by solving the optimization problem

$$c_s\, c_\vartheta \;:\; \min_{c_s,\, c_\vartheta} \left\{ [s_C(\varphi) - s_M(\varphi)]^2 + [\vartheta_C(\varphi) - \vartheta_M(\varphi)]^2 \right\} \;. \tag{25}$$

Thus, one obtains a method for determining an actuation of a compliant two-degree-of-freedom mechanism from geometric measurements.

4 FITTING OF MODEL PARAMETERS TO ANATOMIC DATA

Fitting of model parameters to anatomic data consists of two basic steps. In a first step, the geometric parameters are obtained from static x-ray measurements of the forearm. In a second step, the stiffness coefficients of the two virtual springs are determined from a motion measurement such that swaying angle and dislocation at the humero-ulnar articulation correspond to the computed values, using the optimization procedure of Eq. (25). In the present study, fitting of geometric and swaying angle data were performed *in vivo* by x-ray and magnetic resonance imaging (MRI) measurements, respectively, while the dislocation was fitted using *in vitro* measurements on a cadaveric probe. Based on this model, in future also complete *in vivo* data fitting is conceivable by geometric measurements under physiologic loading conditions.

4.1 Geometric parameter fitting using x-ray measurements

The purpose of geometric data fitting is to determine the link lengths of the surrogate forearm mechanism through x-ray measurements. In this setting, a simple procedure for determining the model paramters r_1, r_2, r_3, r_4 of the surrogate mechanism is required, such that it can be applied easily in practice. To this end, the basic assumption $r_1 = r_3$ and $r_2 = r_4$ is made. This corresponds to the basic assumption that the surrogate mechanism is a parallelogram in the supination configuration. From x-ray measurements, it is easy to determine the distance ℓ_{dia} from the proximal point of the head of the radius to the distal point of the styloid process of the ulna (see Fig. 7). Due to the small ratio of offset values r_2 and r_4 with respect to the bone lengths r_1 and r_3, respectively, this length differs only by second order terms from the actual

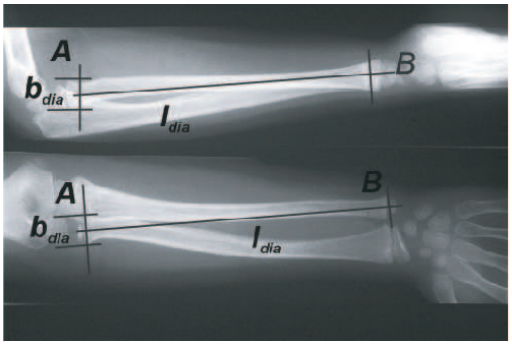

Figure 7: Identification of geometric parameters from orthogonal x-ray measurements

bone lengths. Thus, for a first approximation, the distance ℓ_{dia} can be set equal to the lenghts r_1 and r_3. Another quantity easy to determine from x-ray measurements is the diameter b_{dia} of the head of the radius, which is the largest diameter of the head of the radius perpendicular to the axis of the neck of the radius. This radius was found to be roughly equal to the offsets r_2 and r_4 (see Fig. 7). Thus, for a first approximation, one can set $r_2 = r_4 = b_{\text{dia}}$. Alltogether, the procedure described above presents a simple method for fitting the geometric parameters of the surrogate mechanism to anatomic data, which can be easily applied in medical practice.

4.2 Kinetostatic parameter fitting

In order to determine the stiffness coefficients of the virtual springs, one requires a measurement of the swaying motion of the ulna as well as a measuremt of the axial translation at the humero-ulnar joint. For the swaying motion, a MRI measurement of the bone motion was carried out with a voluntary. Fig. 8 shows the chosen slices for a right arm of the test person. The

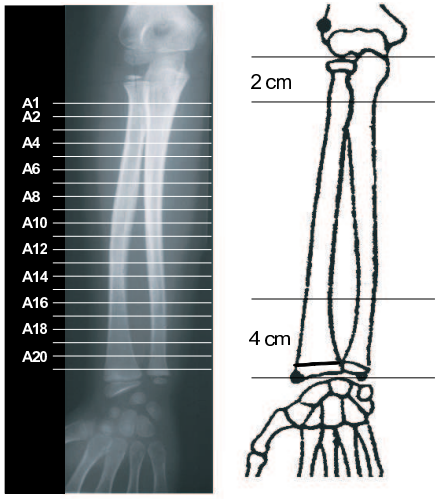

Figure 8: Location of MRI slices for the right arm

pronation motion was carried out with the elbow flexed at 35°, with the upper arm fixed by plaster, and the hand of the volunteer holding a horizontally hinged rotation indicator for measuring the pronation angle. Shown in Fig. 9 are the resulting measurements from the perspective of the wrist. The three rows, from top to bottom, display the ensuing measurements for the slices $A5$,

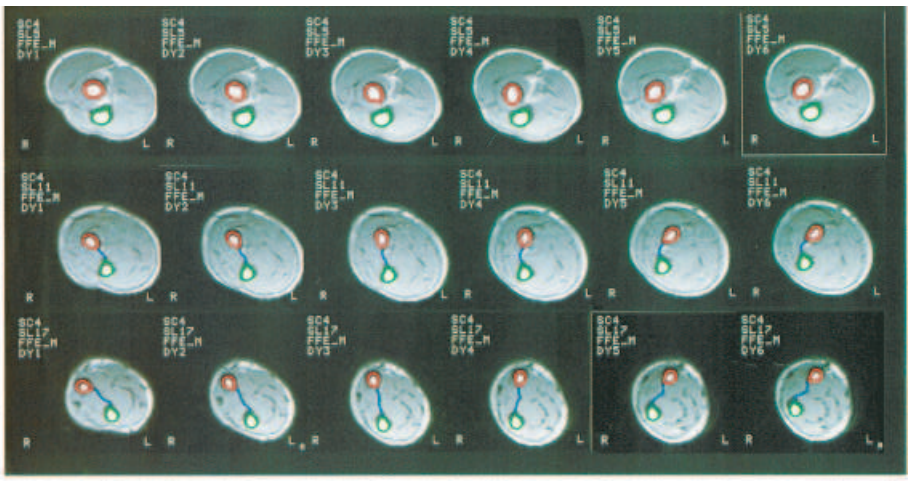

Figure 9: MRI measurements for slices A5, A11 and A17.

$A11$ and $A17$, respectively, where $A5$ is nearer to the elbow and $A17$ is nearer to the wrist. The individual columns show, from left to right, the resulting measurements for the transition from supination ($\varphi = -30°$) to pronation ($\varphi = 45°$) in steps of 15°. Each slice displays the soft tissue (grey area) as well the cross sections of the radius (upper small circle) and the ulna (lower small circle). The dark line connecting both cross sections represents the membrana interossea. As it can be seen, near the elbow (upper row) the cross sections corresponding to ulna and radius are basically fixed, while near the wrist (lower row) a clear motion of both cross sections occurs. The pronation angle is roughly reproduced by the angle between the membrana interossea and the horizontal direction. Clearly, the ulna performs a lateral displacement to the external (here the left) side. This coincides with the model assumption that there is a rotational degree of freedom at the humero-ulnar articulation perpendicular to the elbow flexion/extension axis which allows the ulna to sway to the lateral side as the forearm is rotated from supination to pronation.

For the dislocation motion, a test-bed was deviced in which a cadaveric arm could be placed such as to measure axial displacement at the humero-ulnar articulation as a function of pro- and supination. Fig. 10 shows the corresponding measurements for three positions (rows) and three loading conditions (columns). The loading conditions were (1) no loading (middle column), (2) loading towards the body (varus stress), and (3) loading away from the body (valgus stress). For each position, the opening at the humero-ulnar joint from ventral view was recorded by a CCD camera. This gap does not represent the axial displacement s at the humero-ulnar joint directly, but comprises also an additional displacement of the edge of the trochleus as a function of the

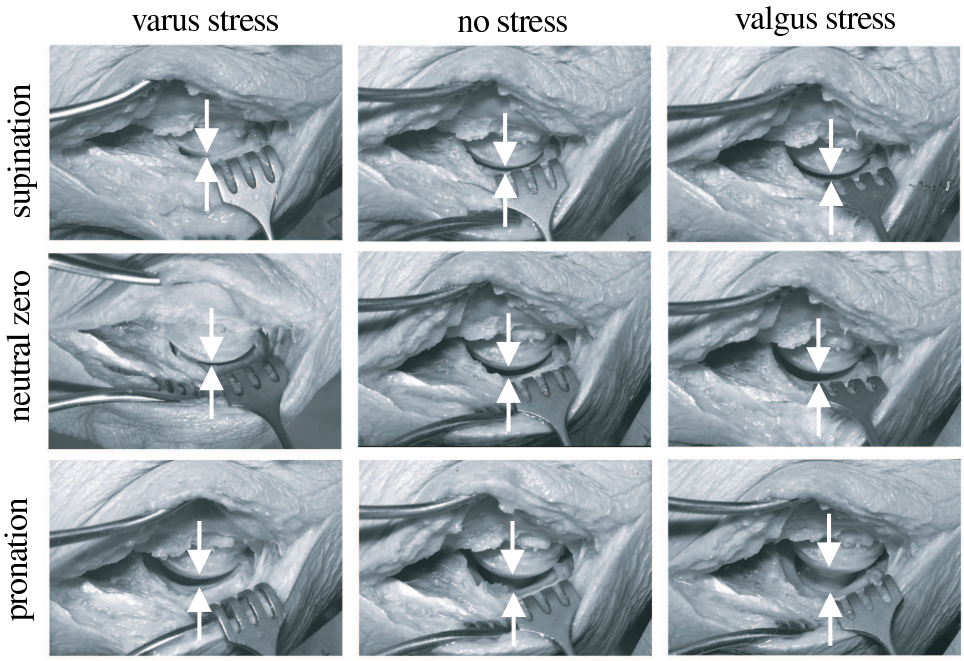

Figure 10: Gap at different pro-/supination configurations

lateral swaying rotation due to the offset between the bone axis and the edge of the trochleus (see Fig. 11). Hence, the observed gap is $\bar{s} = -s + l_o \sin\vartheta + \bar{s}_0$, where $\bar{s}_0$ is a fixed constant relating the model variable s with the measured gap through a fixed offset.

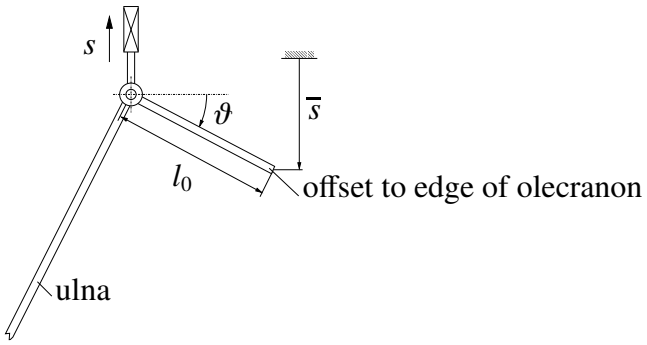

Figure 11: Opening of the gap (pronation)

Using these measurements, the optimization procedure of Eq. (25) was carried out and the values for c_s and c_ϑ were determined. The corresponding numerical values obtained from the measurements and the computations are displayed in Table 1. Hereby, the presented stiffness coefficients do not represent the real absolute values of the stiffnesses induced by the tendon system but scaled quantities, as for the fitting of swaying and axial motion of the ulna only the

ratio of these two coefficients is relevant.

$r_1 = r_3$	$r_2 = r_4$	c_s	c_ϑ	$\vartheta_{\max}$	$\bar{s}_{\max}$
269 mm	25 mm	0.0375 N/mm	11.75 Nmm	7.6°	0.6mm

Table 1: Numerical data for a single-specimen model verification

4.3 Simulation results

Fig. 12 shows the resulting histories of swaying angle ϑ, humero-ulnar gap at the trochlea edge $\bar{s}$, aperture angle ψ_1 and radio-ulnar torsion angle ψ_2 as a function of the pronation angle, respectively. Measured values for swaying angle and gap are shown as small circles. As can

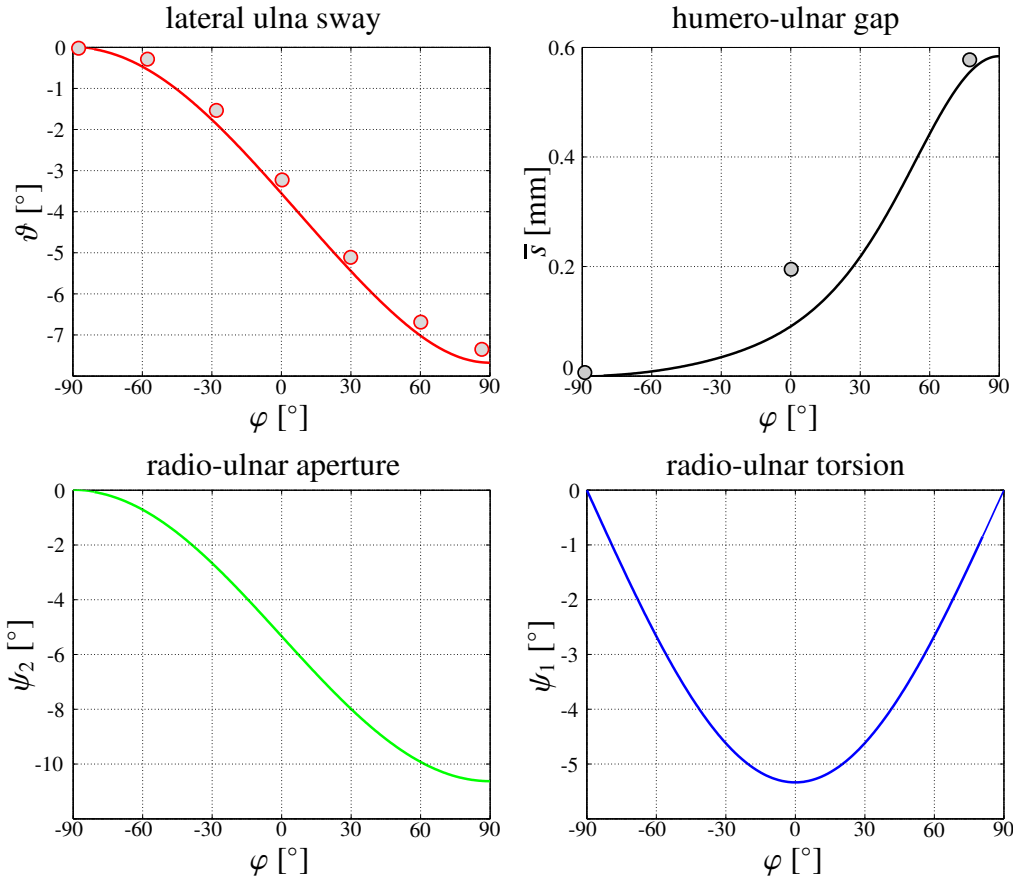

Figure 12: Histories of elbow variables with inserted measured values.

be seen, the model roughly reproduces the measured values. However, these results must be interpreted with caution, as the model fitting was performed in the present case for a single

specimen only. Moreover, there is a discrepancy between experimental data and theoretic model for the humero-ulnar gap at the unloaded position, which stems in the present case from the low resolution of the gap measurement and the use of a cadaveric experiment, which was the only available data source for the present analysis. Nevertheless, the results seem to justify the model assumptions, and hence that the presented surrogate mechanism might be used for more accurate prediction of the forearm pro- and supination motion. Such accurate models may be obtained by performing *in vivo* measurements under different physiologic loading conditions, yielding parametric fields of curves from which the swaying angle, the the gap and the stiffness coefficients can be determined more precisely. This is a topic of further research that is to be tackled in the future.

5 PROGRAMMING ENVIRONMENT

The described model assumptions were implemented using the object-oriented multibody programming library MBILE[18]. In this setting, a bone geometry was imported and attached to the moving frames computed by the multibody code. As a result, one has at disposition a simulating frame in which the pro- and supination motion can be computed online for different values of stiffness coefficients and pronation angle Fig. 13. This online tool allows one to foster

Figure 13: Screenshot of the developed simulation environment for pro-/supination simulation

understanding of the motion properties of pro- and supination and thus could be an important tool for medical training. Moreover, it is intended to generalize the model such that also frac-

tures could be assessed, allowing the surgeon to plan in which way a fracture could be corrected such that possible inhibitations of pro- and supination motion do not occur. It is believed that by the present model such applications may be possible.

6 CONCLUSIONS

In this paper we present a new surrogate mechanism for reproducing pro- and supination motion of the forearm. The mechanism features two degrees of freedom at the humero-ulnar joint that allow the ulna to perform swaying and axial displacements, respectively, as measured in practice. For the determination of the trajectories of the two degrees of freedom, a kineto-static approach is proposed. Here, motion is not computed by pure kinematic transmission, but as a sequence of equilibrium positions under increased loading. The equilibrium positions are controlled by two virtual springs placed at the degrees of freedom whose stiffness coefficients are determined by fitting the simulated motion with the measured motion via an optimization routine. As shown with the simulation results, this fitting renders acceptable agreement between measured and computed values. Thus, the kinetostatic approach provides a new method for matching multi-degree-of-freedom models with geometric measurements, which can be extended to other mechanisms.

ACKNOWLEDGEMENTS

The authors wish to thank Martin Tändl, Daniel Strobach and Gerald Kelz for their support in the programming of the model and the preparation of the figures for this paper.

REFERENCES

[1] E. Jonasch and E. Bertel. *Verletzungen bei Kindern bis zum 14. Lebensjahr*. Hefte zur Unfallheilkunde. Springer-Verlag, Berlin, Heidelberg, New York, 1981.

[2] Ch. Lampert A.-M. Weinberg, H. Reilmann and L. v. Laer. Erfahrungen mit dem Fixateur externe bei der Behandlung von Schaftfrakturen im Kindesalter. *Unfallchirug*, pages 107–113, 1997.

[3] D.J. Fuller and C.J. McCullough. Malunited fractures in children. *J. Bone and Joint Surgery*, 33:364–367, 2000.

[4] J. Oskam, J. Kingma, and H.J. Klasen. Fracture of the distal forearm: Epidemiological developments in the period 1971-1995. *Injury*, 29(5):353–355, 1998.

[5] A.F. Schärli. *Die Frakturen an Unterarm und Hand im Kindesalter*, chapter Operative Therapie diaphysärer Unterarmfrakturen. Universum Verlag, 1995.

[6] A. Menschik. *Biometrie. Das Konstruktionsprinzip des Kniegelenks, des Hüftgelenks, der Beinlänge und der Körpergröße*. Springer-Verlag, Berlin, Heidelberg, 1987.

[7] Andrés Kecskeméthy, C. Lange, and G. Grabner. Object-oriented modeling of multibody dynamics including impacts. In *Proceedings of the European Conference on Computational Mechanics*, pages 1–28, Cracow, Poland, June 26–29 2001. ECCM.

[8] H. Rauber and H. Kopsch. *Anatomie des Menschen (Editors: B. Tillmann, G. Töndury and K. Zille)*, volume I, chapter Ellenbogengelenk. Thieme, Stuttgart, 1986.

[9] I.A. Kapandji. *Funktionelle Anatomie der Gelenke*, volume 1. Enke, Stuttgart, 1999.

[10] R. Fick. *Handbuch der Anatomie und der Mechanik unter Berücksichtigung der bewegenden Muskeln*. Fischer Verlag, Jena, 1904.

[11] Y. Horiuchi T. Nakamura, Y. Yabe. A biomechanical analysis of pronation-supination of the forearm using magnetic resonance imaging: changes of the interosseous membrane of the forearm during pronation-supination. *Nippon-Seikeigeka-Gakkai-Zasshi*, 68:14–25, 1994.

[12] A.-M. Weinberg. *Biomechanische Modellierung der normalen und funktionsgestörten Umwendbewegung des Unterarmes. Habilitationsschrift*. Medizinische Hochschule Hannover. Unfallchirurgische Klinik, 2000.

[13] H. Kerle and M. Frindt. Zur Kinematik eines biomechanischen Modells für den menschlichen Unterarm. In *Getriebetechnik: Warnemünde, 8.–10. September*, pages 115–122. Universität Rostock, Institut für Allgemeinen Maschinenbau, 1997.

[14] M. Helm A.-M. Weinberg, I. Pietsch, J. Hesselbach, and H. Tscherne. A new kinematic model of pro- and supination of the human forearm. *J. Biomechanics*, 33:487–491, 2000.

[15] O. Bottema and B. Roth. *Theoretical Kinematics*. Applied Mathematics and Mechanics 24. North-Holland Publishing Company, Amsterdam, Oxford, New York, 1970.

[16] A. Kecskeméthy and M. Hiller. Automatic closed-form kinematics-solutions for recursive single-loop chains. In *Flexible Mechanisms, Dynamics, and Analysis, Proc. of the 22nd Biennal ASME-Mechanisms Conference, Scottsdale (USA)*, pages 387–393, September 1992.

[17] A. Kecskeméthy. Object-oriented modelling of mechanical systems. In *Kinematics and Dynamics of Multi-Body Systems*, number 360 in CISM Courses and Lectures, pages 217–276, Wien, New York, 1995. Springer-Verlag.

[18] Andrés Kecskeméthy. M⬚BILE1.3 *User's Guide*. Lehrstuhl Mechanik, Universität Duisburg-Essen, 1999.